

Experimental and Numerical Investigation of the Three-dimensional Flow at Expiration in the Upper Human Airways

Franka Schröder, Andreas Lintermann, Michael Klaas, and Wolfgang Schröder

*Institute of Aerodynamics and Chair of Fluid Mechanics, RWTH Aachen University
Willnerstr. 5a, 52062 Aachen, Germany
E-mail: f. schroeder@aia.rwth-aachen.de*

Abstract

This study presents a comparison of numerical and experimental results of the steady flow field in the left main-bronchus of the upper human airways during exhalation. Stereo-particle-image velocimetry measurements were performed in multiple parallel measurement planes for a Reynolds number of $Re_D = 700$ based on the hydraulic diameter of the trachea to determine the highly three-dimensional flow in a realistic transparent silicone lung model. The numerical analysis is based on a Lattice-Boltzmann method. The results for the absolute velocity and the out-of-plane velocity component show a good agreement and emphasize the three-dimensionality of the flow. Two fluid jets, originating from two principal sub-bronchi, predominate the flow in the investigated bronchus. The vortical structures consisting of two pairs of counterrotating vortices are not generated by the curvature of the main-bronchus or the sub-bronchi but are caused by the merging of the flows and the redirection of the jets. Further downstream in the bronchus, the secondary flow structures vanish in the streamwise direction such that no spiral-like flow enters the trachea.

Keywords: multiplane stereo PIV, LBM, steady exhalation, vortical structures.

1. Introduction

Chronic obstructive pulmonary disease (COPD) is not a single illness, it is a collective term to describe chronic lung diseases that cause limitations in lung flow. Patients with COPD complain about breathlessness as the main symptom. According

to the World Health Organization WHO, COPD will be the fourth leading cause of death by the year 2030 [1]. Most of the information about COPD morbidity and mortality is gathered in high-income countries, but 90% of COPD deaths occur in low- and middle-income countries. To lower the morbidity and mortality rate, it is necessary to develop and establish non-invasive medical diagnostic and clinical monitoring of COPD. One possible approach is based on the analysis of exhaled aerosols, since the temporal and spatial distribution of the aerosols as well as the particle size distribution is different for patients with COPD compared to healthy people [2, 3]. Therefore, it is necessary to provide evidence that the flow field in the human lung offers a possibility to transport aerosols from lower generations of the lung to the trachea/mouth to use the exhaled aerosols as biomarkers. For this reason, it is a must to gain detailed information on the highly three-dimensional flow structures in the human airways since these structures determine the particle transport [4, 5, 6, 7].

In the last decades numerous experimental and numerical investigations concerning the flow in the human lung have been conducted. The flow in the human lung is investigated either during a breathing cycle or for steady inspiration and expiration. Investigations dealing with the flow during a breathing cycle are rare and are mostly conducted in symmetric lung models or single bifurcation geometries. A breathing cycle consists of inspiration, expiration, and the corresponding transition points. Zhang and Kleinstreuer [8] showed a good agreement between the results for steady flow and breathing cycles at Womersley numbers $\alpha < 1$, where the Womersley number α defines a non-dimensional frequency. For steady inspiration, multiple experiments and numerical simulations have been conducted dealing with vortical structures. The main focus of these investigations is the particle transport in the lung for drug delivery. Despite many investigations there still exists a considerable uncertainty concerning the complex flow field in the human lung during expiration. This statement holds especially with respect to realistic lung geometries. For realistic models, results are still rare since the human lung is a complex geometric network of bifurcating tubes with an almost arbitrary distribution of decreasing diameters and varying angles.

Fresconi et al. [9] investigated the flow field in a symmetric single-bifurcation for steady and oscillatory flow conditions using particle-image velocimetry (PIV) and laser-induced fluorescence (LIF) and observed secondary flow structures during expiration. The velocity field was measured in five cross-sections and showed a quadruple vortex. At higher Reynolds numbers, the authors observed unsteady flow due to hair-pin vortices that dissolve simultaneously. Considering the results, the authors concluded that particles with small Stokes numbers do not deposit during inhalation and that the particles stay in the bronchial system for several breathing cycles without deposition.

Ramuzat and Riethmuller [10] investigated the time dependent flow field in a plane symmetric model of successive generations of lung bifurcations using two-component/two-dimensional (2C/2D) PIV. Their investigations on oscillating flow phenomena at different Womersley numbers showed the temporal development of the velocity through successive bifurcations and the quasi-steadiness of the flow field at decreasing oscillation frequency.

As mentioned above, the numerical simulations of Zhang and Kleinstreuer [8] for oscillating flow based on a finite volume code for laminar, incompressible airflow in a third-to-sixth-branch Weibel model [11] yielded a good match between steady and breathing-cycle-resolved solutions at Womersley numbers $\alpha < 1$. Due to the geometry of the model, the overall flow field stayed symmetric in all branches. However, especially during expiration secondary flow structures appeared that seem to dominate the aerosol transport and deposition. The authors showed that the inlet velocity profile had less an effect at expiration than at inspiration and that the secondary flow strength was higher in a non-planar model configuration than in the planar configuration during expiration.

Fresconi and Prasad [12] investigated the flow field in a three-generational anatomically accurate but symmetric model of the conducting region of the lung and showed that a critical Dean number of 10 had to be exceeded for the formation of vortices. Their PIV measurements confirmed that the oscillatory flow field hardly differs from the corresponding steady flow field up to a Womersley number $\alpha < 1$.

To overcome the restrictions of planar data sets and two-dimensional results, e.g., vector fields, Soodt et al. [5] performed stereo scanning PIV measurements for the transition from inspiration to expiration in the right main-bronchus and the subsequent lobe bronchi at two Womersley numbers in a realistic lung model consisting of the bronchial tree up to the third bifurcation. The measurements showed an increased mass flux into the right superior bronchus at the higher Womersley number, frequency-dependent phase shift of the flow structures, and a heterogeneous outflow at the beginning of the expiration phase.

Adler et al. [13], Bauer et al. [14], and Adler and Brücker [15] concentrated on the flow field in a six generation model based on the geometry of Horsfield et al. [16] for the trachea and the first bifurcation and that of Weibel for the second to the sixth generation. 2C/2D PIV measurements and numerical simulations were performed to investigate the velocity field in different cross-sections for two phases of a breathing cycle. On the one hand, the authors investigated maximum inspiration and expiration. On the other hand, they focused on the transition from inspiration to expiration and vice versa. An asymmetric velocity profile at the end of inspiration was observed at higher Womersley numbers. The numerical simulation of the identical geometry revealed that the flow structures at expiration mainly depend on the curvature and orientation of the branches and that they are almost independent of the adjacent upper and lower generations. The vortical structures in the bronchial system are regenerated at each bifurcation such that these vortices, which are known as Dean vortices [17, 18], were found in each branch of this simplified geometry.

Martonen et al. [19] simulated the flow field in a two-bifurcation model for inspiration with a finite element method for incompressible, isothermal, laminar and steady flows. The authors pointed out that secondary flows were stronger at the beginning of the daughter tubes and that their intensity decreased in the downstream direction. Furthermore, the secondary motion became stronger at increasing Reynolds number or bifurcation angle.

Van Ertbruggen et al. [20] presented numerical results based on a finite volume method for laminar, incompressible airflow for a realistic lung model based on the

model of Horsfield et al. [16] and on bronchoscopic and CT-images, which define the spatial geometry of the curved branches. The results evidenced the highly three-dimensional character of the flow field emphasizing the importance of non-fully developed flows for inspiration in the branches due to their short length.

Experimental results of 2C/2D PIV measurements in 13 parallel measurement planes in the left main-bronchus were presented by Große et al. [21, 22]. A pair of counterrotating vortices was observed in the left bronchus during inspiration and the flow field consisted of complex vortical structures for both transition phases, i.e., from inspiration to expiration and vice versa. For steady inspiration and expiration experimental findings of Große et al. [21, 22] showed a good agreement with numerical simulations by Freitas and Schröder [23] that were based on the Lattice-Boltzmann-Method. The numerical and the experimental findings contained very intricate flow structures for expiration, where the complex pattern in the trachea is a consequence of the asymmetric merging of the two flows coming from the left and right principal bronchus.

Eitel et al. [4] concentrated their experimental and numerical investigations on secondary vortex structures and their temporal development in the center plane of the first two bifurcations of a realistic lung geometry up to the sixth generation. Their results evidenced a more homogeneous velocity distribution for expiration than for inspiration. Secondary flow structures known from steady state simulations for inspiration were clearly identified and the pair of counterrotating vortices as well as the high-speed region observed by Große et al. [21, 22] were confirmed.

This discussion shows that there is a lack of detailed investigations of the three-dimensional flow field during expiration, which are essential to analyze particle transport during expiration. To get a deeper insight into the flow structure in the upper bifurcations, i.e., to determine whether or not pronounced vortical structures exist at expiration, it suffices to analyze the flow at steady-state conditions for Womersley numbers $\alpha < 1$. For this reason, an experimental and numerical investigation in a realistic three-dimensional lung geometry is performed. The steady flow possesses a Reynolds number $Re_D = 700$, which is the Reynolds number at maximum expiration during a recorded breathing cycle of a patient for normal breathing at rest. The focus of the analysis is on the three-dimensional flow field in the left main-bronchus being the longest branch such that three-dimensional structures can develop over an extended length. The question pursued in this study is whether there is a vortical flow structure in the bronchus and if so what is the origin of this flow pattern. To tackle this problem, detailed experimental and numerical analyses are conducted.

The paper is organized as follows. First, the flow problem, the experimental setup, and the numerical method are described. Then, the experimental results are discussed and compared to the numerical findings for steady expiration. Finally, conclusions are drawn.

2. Flow Problem and Experimental Setup

The flow in the left bronchus of the human lung can be described as the flow through a pipe bend. The dimensionless parameter to characterize the flow in pipe bends is the

Dean number [17, 18], which can be considered as the Reynolds number scaled by the curvature of the pipe. The Reynolds number reads

$$Re = \frac{\rho U D_h}{\mu}$$

where ρ and μ denote fluid density, dynamic viscosity of the fluid, volume flux, and the hydraulic diameter. The Reynolds number of this study is based on the hydraulic diameter of the trachea and the maximum bulk velocity corresponding to a volume flux in the trachea of .

The Dean number describes the ratio of the viscous forces to the centrifugal forces acting on the fluid in a pipe bend. The Dean number reads

$$Dn = Re \sqrt{\frac{r}{D_h}}$$

where Re is the Reynolds number, D_h the hydraulic diameter of the bronchus, and r the radius of the curvature of the bronchus. In the current analysis, the Dean number is based on the mean curvature between the main-bronchus and the trachea. The curvature has been extracted from the STL-data of the lung model. The Reynolds number in the bronchus equals based on the diameter of the bronchus . Note that investigations by Agrawal et al. [24] and Humphrey et al. [25] showed that a pair of counterrotating vortices occurs in a u-shaped pipe for which is somewhat higher than the Dean number in this study.

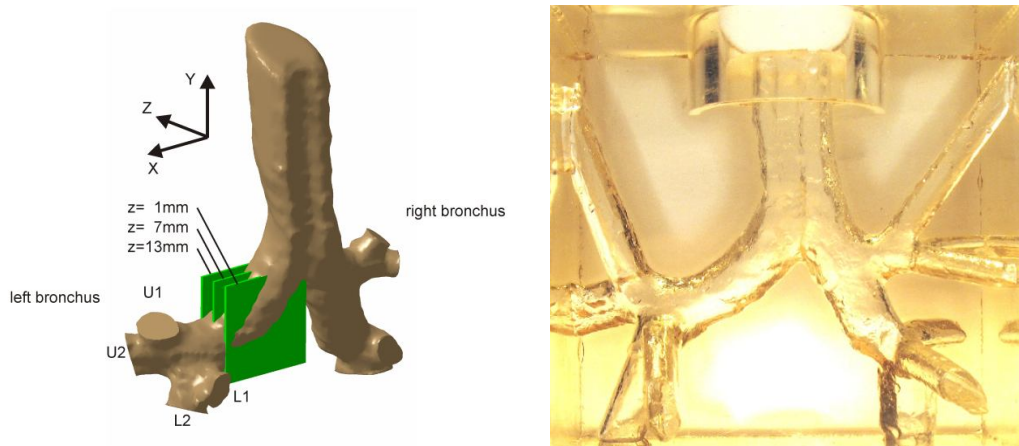


Fig. 1: Overview of the lung model. Left: Dorsal view of the CAD model of the lung showing the measurement planes in green. Right: Dorsal view of the silicone model.

The fully transparent, three-dimensional, realistic lung model shown in Fig. 1(a) comprises the trachea, the first, the second, and the third generation of the geometry of the upper human lung of a healthy patient. To generate the model, a post processing of the CT-data including digital geometry reconstruction, segmentation, surface generation, and surface smoothing is performed. The CAD data are used to produce a

kernel made from corn starch which is embedded in liquid silicone and washed out after the silicone has dried. The extensions of the model's exits to the outer edge of the silicone cast are drilled such that they can be considered as straight extensions of these branches.

The model is made from the two component PDMS RTV 615 to allow perfect optical access, see Fig. 1(b). In this region of the lung, i.e., the trachea and bronchi, the flexibility of the airways can be neglected, as already assumed in earlier investigations of Soodt et al. [5] and Große et al. [21, 22]. Taking the trachea as the zero bifurcation, the trachea first splits to form the left and right bronchi (first bifurcation). The left bronchus then divides into the bronchioles of the upper and lower left pulmonary lobes (second bifurcation). The right bronchus bifurcates into the bronchioles of the lower right pulmonary lobe and the subdivision containing both the upper right and center right pulmonary lobes (second bifurcation). The center right pulmonary lobe then bifurcates a second time to form the bronchioles of the center and lower lobes (third bifurcation). The labeling of the branches is given in Fig. 1(a). The lobes are indicated by the letters "U" and "L", whereby "U" stands for upper and "L" for lower lobe. The bronchioles closer to the trachea are labeled as "1" and the more distant ones as "2".

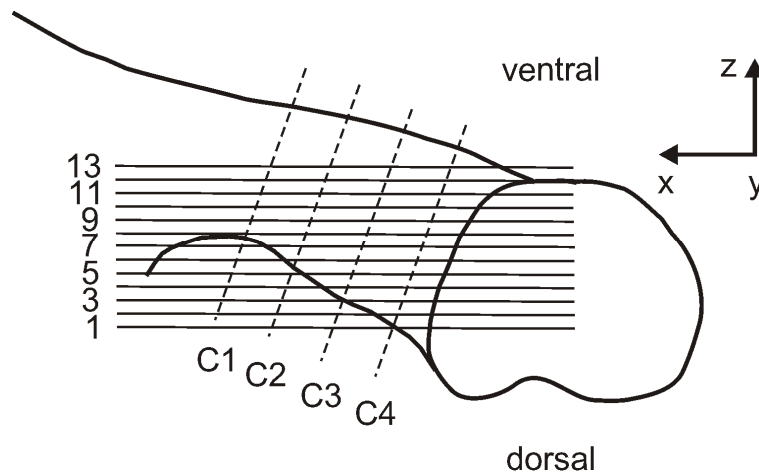


Fig. 2: Location of the 13 parallel measurement planes and the normal cross sections C1, C2, C3, and C4 in the left main-bronchus.

The measurements have been performed in the left bronchus of the first bifurcation such that the spatial evolution of the merging fluid flows from the adjacent bronchi via the inlets "U1", "U2", "L1", and "L2" as illustrated in Fig. 1(a) could be investigated.

The positions of the measurement planes are shown in Fig. 1(a) for three representative measurement planes. The plane $z = 7\text{mm}$ is aligned with the center of the trachea. The other two measurement planes are positioned closest to the outer and inner wall, respectively, and each has a spatial distance to the center plane of $\Delta z = 6\text{mm}$. For better illustration, only these three of the overall 13 measurement planes are depicted in the sketch.

To ensure optical access without distortions, a refractive-index matching fluid is used. By changing the ratio of water (39 mass percent) and glycerin (61 mass percent),

the refractive index of the measurement fluid is adapted to that of PDMS at an accuracy of $\Delta n = 1 \cdot 10^{-3}$. The refractive-index of the silicone block and the test fluid were experimentally measured by an Abbe refractometer and estimate to a value of $n = 1.411$. According to Cheng [26] the water/glycerin mixture has a dynamic viscosity of $\eta = 9.91 \cdot 10^{-3} Pa \cdot s$ and a density of $\rho = \frac{1127.86 kg}{m^3}$ at a temperature of $T = 297 K$ during the experiments.

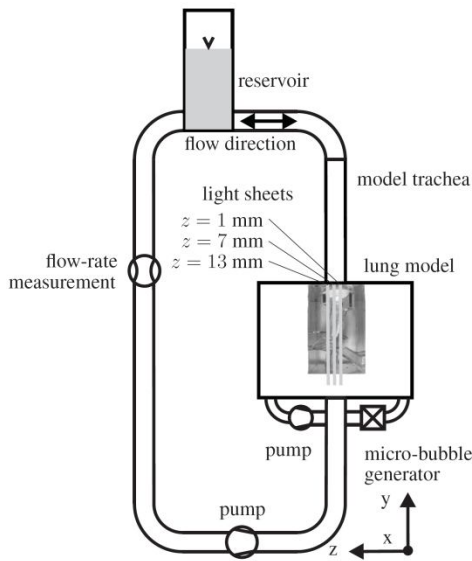


Fig. 3: Schematic of the experimental setup for steady flow showing three representative measurement planes (1 mm, 7 mm, 13 mm).

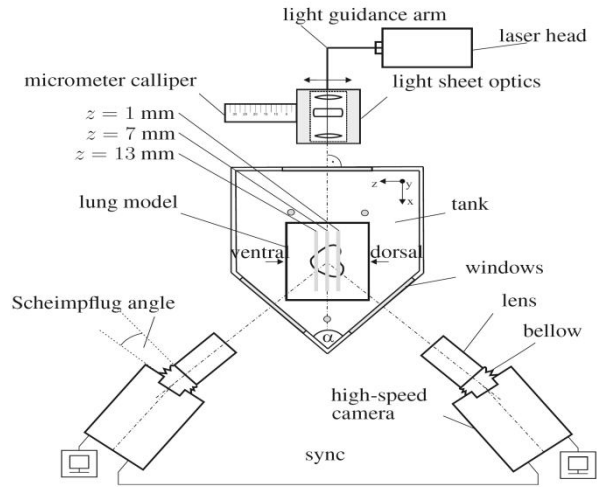


Fig. 4: Top view of the optical setup with three representative measurement planes (1 mm, 7 mm, 13 mm).

The experimental facility is built such that the model can be embedded either in a closed circuit for steady expiration or in an open-circuit flow for oscillating flow [5]. For the simulation of expiration a constant working pump is used to generate a homogeneous flow as shown in Fig. 3. Since a homogeneous flow circulation has to be guaranteed for an idealized flow distribution in the lung model, the fluid supply was carefully designed to minimize any perturbations on the flow field.

Air-bubbles generated by a micro-bubble generator based on the Venturi mechanism [27] are used as tracer particles. Due to the deposition of solid particles on the inner surfaces of the model resulting in strong reflections at the boundaries of the bronchial system and as such in a significantly reduced quality of the images, the use of air-bubbles was necessary. To achieve a homogenous seeding distribution, the micro-bubble generator is placed inside a second circuit and connected to the bottom of the measurement tank. The air flow rate as well as the air pressure are carefully chosen and kept constant for all experiments to achieve a constant particle size for all experiments. The particles have a median diameter of about $d_p = 11.9 \mu m$ based on Interferometric Particle Imaging (IPI) measurements. The concept of IPI is given by

König et al. [28] and more detailed descriptions can be found in Albrecht et al. [29] and Semidetnov and Tropea [30].

All experiments are conducted using the multiplane-stereo PIV system shown in Fig. 4. The PIV setup consists of two Fastcam PCI 1024 cameras operating at 60 frames per seconds and a Quantel Twins BSL 140 laser at a wavelength of $\lambda = 532 \text{ nm}$. The angle between the two cameras is 100° to guarantee constant path lengths from the object plane to the image plane and as such to keep the image perpendicular to the optical axis and fulfill the Scheimpflug criterion. The light sheet optics generated a light sheet with a thickness of 0.7 mm and was mounted on a micrometer calliper to guarantee the position- ing and movement in 1 mm steps. The PIV image dimensions were $73 \text{ mm} \times 58 \text{ mm}$ and adaptive cross correlation with a final window size of 16×16 pixels was used. The overlap of 50% led to a final vector spacing of $\delta_x = 1.15 \text{ mm}$.

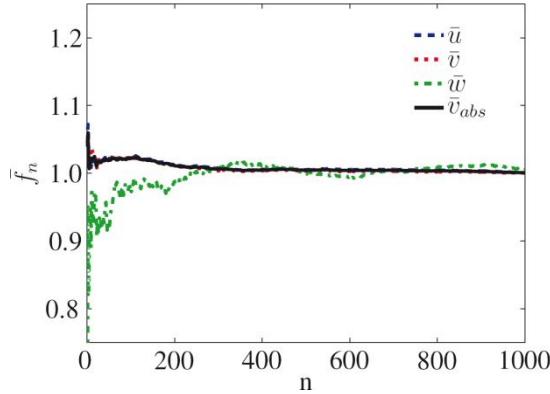


Fig. 5: Calculation of the running mean \bar{u}_n , \bar{v}_n , \bar{w}_n and $\bar{v}_{abs,n}$ for the velocity components at 1000 PIV data sets for one single point in center of the left bronchus.

At steady expiration 400 pairs of independent images were captured to determine the flow structures. Fig. 5 shows the results for the normalized running mean of various quantities. The normalized running mean is defined as

$$\bar{f}(n) = \frac{1}{n} \sum_{n=1}^n f$$

$$\bar{f}_n(n) = \bar{f}(n) / \bar{f}(1000)$$

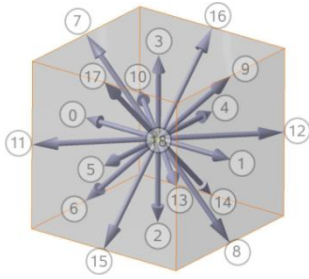
where f represents a random variable and n the number of images. The values are calculated for one single point in the center of the investigated bronchus and normalized by the mean value for 1000 data sets. The velocity components u and v are the in-plane velocity components in the measurement planes in the x - and y -direction and w is the out-of-plane component. The absolute velocity is calculated by $v_{abs} = \sqrt{u^2 + v^2 + w^2}$.

The running mean of the corresponding velocity components \bar{u}_n , \bar{v}_n and $\bar{v}_{abs,n}$ converge after an average of 300 pictures where the running mean of the out-of-

plane component \bar{w}_n shows a slightly poorer convergence rate. Nevertheless, at approximately 400 images an almost constant value is reached which is why 400 images were used for the analysis of the flow structures.

3. Numerical Method

The numerical simulations were performed using a highly parallel Lattice-Boltzmann (LB) code. The LB method has been validated by canonical test cases [31] and has been proven to be well suitable for bio-mechanical flow problems in moderate Reynolds number regime, e.g., for flow simulations in the human airways [4, 23].



$$\xi_i = \xi_0 \begin{cases} (\mp 1, 0, 0); (0, \mp 1, 0); (0, 0, \mp 1) & \alpha = 0 \dots 5 \\ (\mp 1, \mp 1, 0); (\mp 1, 0, \mp 1); (0, \mp 1, \mp 1) & \alpha = 6 \dots 17 \\ (0, 0, 0) & \alpha = 18 \end{cases}$$

Fig. 6: D3Q19 model for phase space discretization.

The LB code in this study is solving the Bathnagar-Gross-Krook (BGK) equation [32, 33]

$$f_i(\vec{x} + \xi_i \delta t, t + \delta t) = f_i(\vec{x}, t) + \omega \delta t (f_i^{eq}(\vec{x}, t) - f_i(\vec{x}, t)) \quad (1)$$

for the particle probability distribution functions f_i (PPDFs) in three dimensions in 19 directions with the D3Q19 model by Qian et al. [34] as shown in Fig. 6. The PPDFs represent the probability to find a certain particle at a velocity ξ_i at a location \vec{x} in phase space. Equation (1) describes a relaxation towards a thermodynamical equilibrium given by the discretized Maxwellian distribution function

$$f^{eq}(x_\alpha, t) = \rho t_p \left[1 + \frac{v_\alpha \xi_\alpha}{c_s^2} + \frac{v_\alpha v_\beta}{2c_s^2} \left(\frac{\xi_\alpha \xi_\beta}{c_s^2} - \delta_{\alpha\beta} \right) \right], \quad (2)$$

scaled by the molecular collision frequency

$$\Omega = \omega \delta t = \frac{c_s^2 \delta t}{v + 1/2 c_s^2 \delta t}, \quad (3)$$

which depends on the kinematic viscosity ν and the speed of sound $c_s = (1/\sqrt{3})(\delta x/\delta t)$. The quantities δx and δt define the space and time step, $v_{\alpha,\beta}$ the local velocities, $\delta_{\alpha,\beta}$ is the Kronecker delta with $\alpha, \beta \in \{1, 2, 3\}$, and ρ is the density. The

weighting factors t_p are direction dependent and are based on the discretization model. Equation (1) is solved iteratively in two steps. First, the collision step, represented by the right-hand side, is performed. Subsequently, the newly generated information is propagated to the neighboring cells, i.e., the operation on the left-hand side of Equation (1) is conducted. The macroscopic variables are obtained from the moments of the PPDFs listed in Table 1.

Table 1: Moments of the PPDFs.

Variable	Discrete Moment
Density	$\rho = \sum_{i=0}^{18} f_i = \sum_{i=0}^{18} f_i^{\text{eq}}$
Momentum	$\rho v_a = \sum_{i=0}^{18} \xi_{i,\alpha} f_i = \sum_{i=0}^{18} \xi_{i,\alpha} f_i^{\text{eq}}$

According to the experimental setup, an outlet pressure boundary condition was applied at the trachea yielding a Reynolds number of $Re_D = 700$. At the inlets a Saint-Venant/Wanzel condition [35, 36] is applied prescribing the pressure based on the local momentum. For the velocities a von Neumann condition is used. The no-slip wall boundary condition is based on the interpolated bounceback modeling for inclined walls [37].

The computational mesh was generated using a massively parallel Cartesian grid generator. The mesh has a resolution of $11.75 \times 10^{-2} \text{mm}$ and consists of approximately 40×10^6 cells. The simulation was conducted on the CRAY XE6 Hermit at the High Performance Computing Center Stuttgart (HLRS) on 256 AMD Opteron 6276 (Interlagos), i.e., on 4096 cores. The converged state was reached after 10^5 iteration steps.

4. Results

The scope of this study is to analyze the three-dimensional flow structures in the left bronchus of the upper human airways during expiration. The results are based on PIV measurements in 13 parallel planes whose locations are defined in the experimental setup section (see Fig. 1(a) and 2). The Lattice-Boltzmann results complement the measurements in the sense that additional data between the experimental planes are available to analyze the flow structures.

The following hypothesis is analyzed in this study. The Dean number $De = 140$ is below the necessary value to generate vortical flow structures in the bronchus [24, 25]. However, it is not only the volume flux and the curvature of the bronchus that defines the flow pattern, but also the flow injected through the inlets upstream of the bronchus. The jets at these inflow cross-sections cause vortical structures in the bronchus that determine the wash-out mechanism during expiration even at a relatively low Dean number.

In Fig. 7 and 8 the Lattice-Boltzmann solutions (top) and the multiplane-stereo particle-image velocimetry data (bottom) for steady exhalation at a Reynolds number of $Re_D = 700$ are juxtaposed. Fig. 7 gives a general overview of the flow field based on contours of the absolute velocity v_{abs} distribution. A more detailed comparison of the flow field in the left bronchus during exhalation is shown by the out-of-plane component w in all measurement planes in Fig. 8 to emphasize the three-dimensional flow character.

In the overview illustrated in Fig. 7, the merging of the jet-like flow through the "U1", "U2", "L1", and "L2" inlets shown in Fig. 1(a) can be observed. Note that the investigated planes are not parallel to the orientation of the bronchus (see Fig. 2) such that over the length of the plane the location within the bronchus changes and different flow structures are captured.

The measurement planes will be discussed from dorsal to ventral (measurement plane 1 to 13) where the outside of the bronchus is the lower curvature and the inside of the bronchus is the upper curvature. In the measurement planes several jet-like flows with different origin can be observed. In the measurement planes $z = 1\text{mm}$ and $z = 2\text{mm}$ the flow of the inlets "L1" and "L2" can be seen. The flow of both inlets has already mixed since these two measurement planes are located at the outlet of the bronchus near the trachea.

In the measurement planes $z = 3\text{mm}$ to $z = 5\text{mm}$ two flow structures can be detected. Both of them originate from the mixed fluid. The upper one is mixed fluid from the inlets "L1", "L2", and "U1", whereas the lower one is from "L1" and "L2". It can be assumed that vortical structures exist in this bronchus since mixed fluid of the "L1" and "L2" inlet can be detected in both flow structures.

Near the center of the bronchus in measurement planes $z = 6\text{mm}$ to $z = 8\text{mm}$ it is hard to distinguish where the fluid originates from. The lower jet at the outside still seems to be a mixture of "L1" and "L2", but unlike to the measurement plane discussed above the fluid in the upper part at the inside originates only from the "U1" inlet.

In the following measurement planes starting from measurement plane $z = 9\text{mm}$ two jet-like structures at the entrance of the bronchus can be clearly assigned. The lower one at the outside originates from the "L2" inlet and the upper one from the "U1" inlet. The streams merge and half way into the bronchus the two-jet structure is no longer visible due to the pronounced mixing.

Since the measurement planes are located in the center of the bronchus in the upstream direction, the impact of the flow via the "U2" inlet cannot be detected in the area investigated in the experiments. In general, the experimental and numerical results in Fig. 7 are in good agreement considering the overall structure of the flow field. Nevertheless, there are some differences, which need to be discussed. The high speed regions in planes $z = 11\text{mm}$ to $z = 13\text{mm}$ are considerably smaller in the experimental than in the numerical results, and the near wall resolution in the experimental data is smaller than in the numerical simulation due to laser light reflection. The reason for this reflection is that the upper area of the light sheet is in very close vicinity to the inner sidewall of the bronchus since the bronchus shown in Fig. 1(a) possesses a significant curvature at the bifurcation between trachea and left

bronchus. Furthermore, the experimental results suffer from too few particles in the near-wall region which is why the flow structures cannot be resolved in this vicinity of the walls.

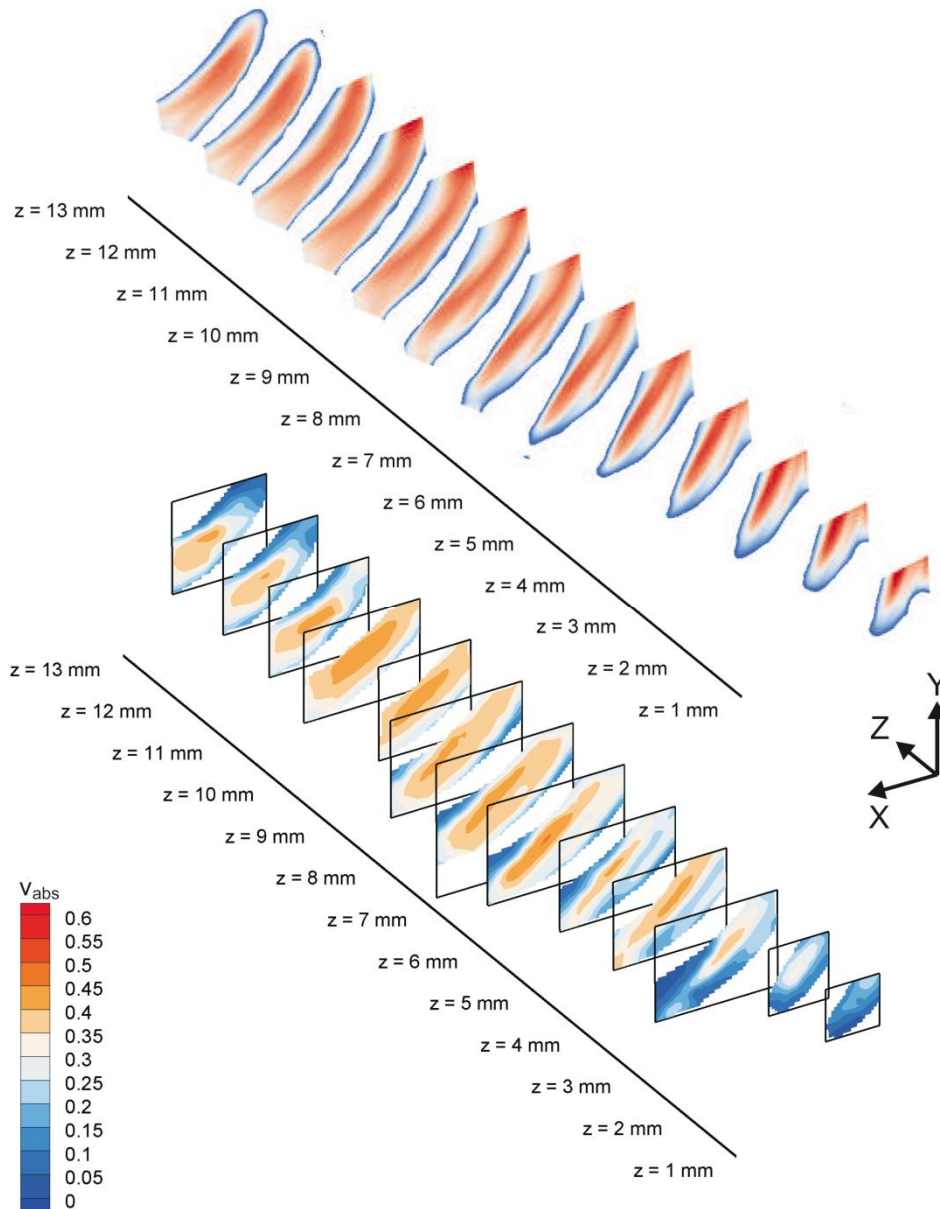
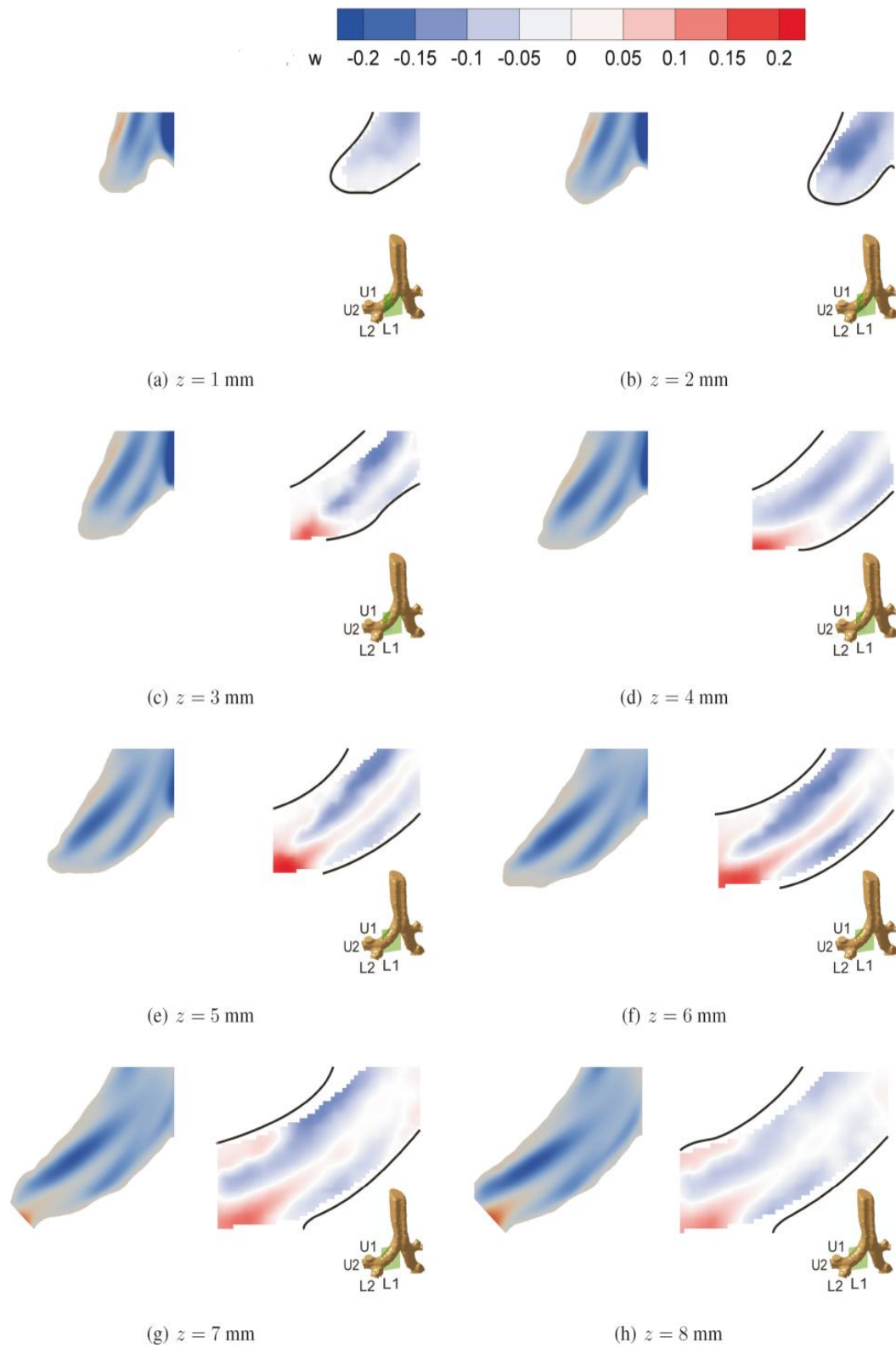


Fig. 7: Absolute velocity distribution v_{abs} in the left main-bronchus for steady expiration in 13 parallel planes; numerical results (top) and experimental results (bottom).



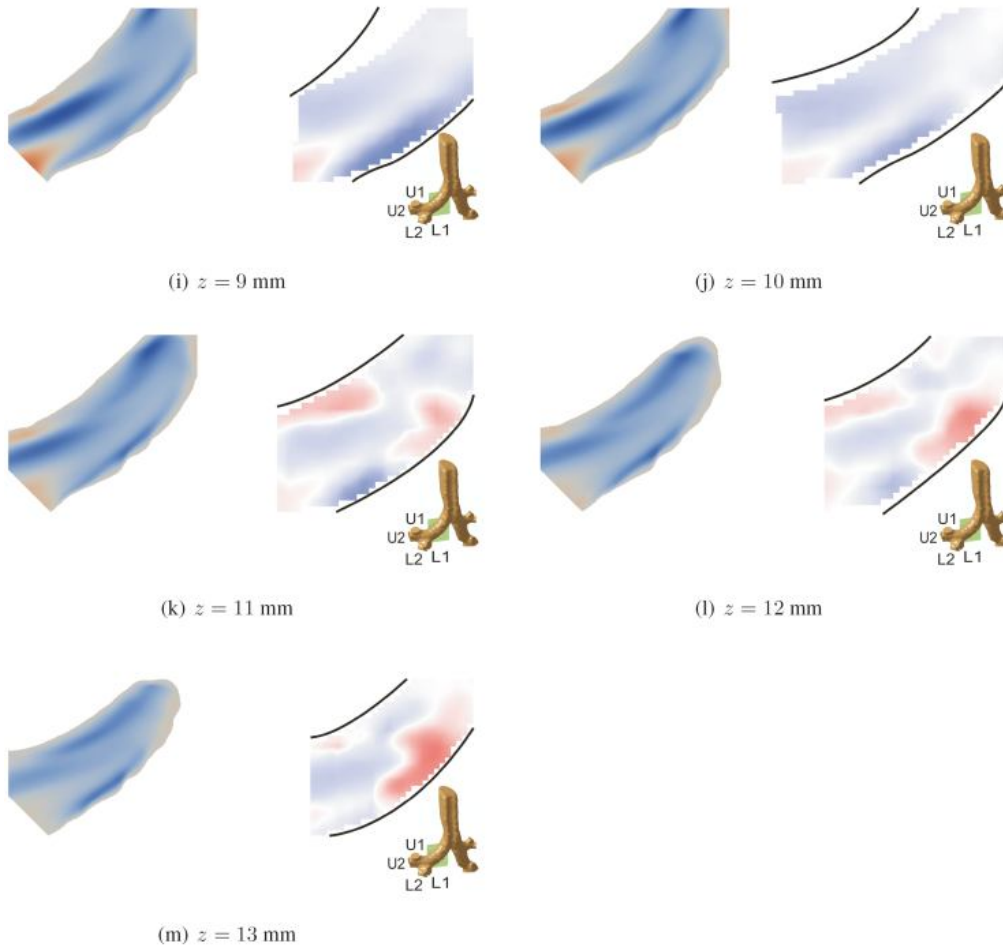


Fig. 8: Distribution of the out-of-plane velocity w ; the position of the measurement plane is shown in the schematic; numerical results (left) and experimental results (right).

The illustration of the out-of-plane velocity component w in Fig. 8 yields a more detailed view of the three-dimensional flow structures in the left bronchus. Note that the order of magnitude of this velocity component is comparable to that of the in-plane velocity components u and v . To be more precise, its maximum and minimum values are approximately one third of the in-plane components.

Again, a complete three-dimensional reconstruction of the measured flow field is not possible due to the reflections of the wall of the model.

In all measurement planes relatively high negative out-of-plane components can be detected. The corresponding positive out-of-plane component is smaller in value and spatial distribution than the negative component.

Since the merging flow of the subbronchi "L2" and "U1" dominates the flow in the bronchus, the vortical structure of these will be discussed first. In the measurement planes $z = 11 \text{ mm}$ to $z = 13 \text{ mm}$ the results of the PIV measurements and the simulations are similar at the beginning of the bronchus. The numerical results and the experimental data possess high out-of-plane components at the upstream end of the

bronchus (Fig. 8(k)-8(m)). Due to the geometry it can be assumed that the lower flow undergoes a stronger redirection compared to the fluid in the upper part of the bronchus. The lower fluid enters through the "L2" subbronchus and the upper flow through the "U1" subbronchus. The signchange of the out-of-plane component at the inlet of the bronchus and further downstream indicates the spiral-like structure of the flow in the streamwise direction.

The measurement planes $z = 7mm$ to $z = 11mm$ show a high out-of-plane component in the lower left corner. It is in this area where the jets from the subbronchi "L1" and "L2" possess their most pronounced effect. In other words, this mixing of the jets from "L1" and "L2" is the origin of the spiral-like motion in the bronchus. In the upper part of the bronchus, the fluid from the subbronchus "U1" mixes with fluid from "L1" and "L2".

The positive out-of-plane component near the upper wall is evidenced in the numerical results. This distribution of the out-of-plane component over the whole cross section confirms the existence of counterrotating vortices. This flow structure is also in agreement with both the numerical and experimental results in the planes $z = 3mm$ through $z = 7mm$.

In the planes $z = 4mm$ to $z = 9mm$ in the center of the bronchus at the lower near-wall region an additional negative out-of-plane component can be observed. In comparison with the v_{abs} -results, this component is caused by the flow from bronchus "L2" flow. This leads to the assumption that a third vortex occurs approximately one third downstream of the bronchus. This vortex is not as strong as the counterrotating vortex pair induced by the flow from the bronchus "U1" and mixed fluid from the bronchi "L1" and "L2" and vanishes in the streamwise direction.

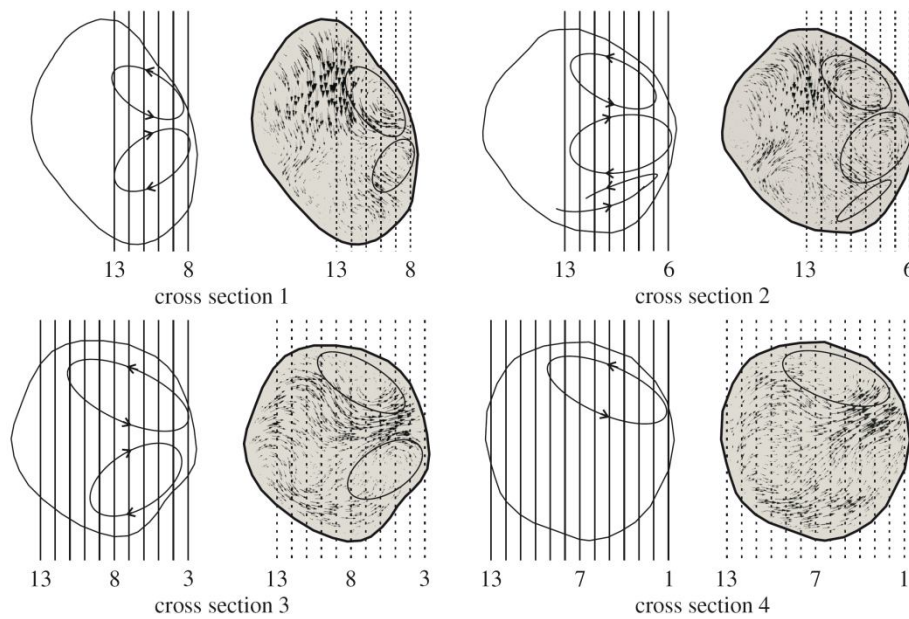


Fig. 9: Left-hand side: Schematics of the flow structure in the left main-bronchus. The solid lines indicate the measurement planes. Right-hand side (shaded area):

Corresponding cross sections from the numerical simulation. Dotted lines show the location of the corresponding measurement planes in the experiments.

All thirteen planes show that the vortical structures have vanished at the end of the bronchus and vortical structures which appear in the trachea are generated anew, based on the curvature between bronchus and trachea.

The schematics in Fig. 9 show a reconstruction of the flow field based on the experimental results (left) perpendicular to the streamwise direction in the cross sections which are defined in Fig. 2 and the results of the numerical simulation in the corresponding cross sections (right). Note that cross section 1 is located most upstream in the left bronchus. The pair of counterrotating vortices generated by the jets from the bronchi "U1" and "L1" is sketched in cross section 1. The third vortex induced by the flow from bronchus "L2" is located below the two vortices and near the wall of the bronchus. This structure is detected only in cross section 2 since the vortex is weaker than the counterrotating pair and vanishes further downstream. In cross section 3, the intensity of the lower vortex is less than the intensity of the upper vortex. The strength of this vortex diminishes in the streamwise direction but it is still detectable in cross section 4. In summary, the flow field consists of a counterrotating vortex pair whose strength is primarily determined by the jets "L1" and "U1". Due to the varying strength of the jets, the counterrotating vortices possess a different strength which decreases in the streamwise direction.

Since the numerical simulation provides three-dimensional data, it can be used to gain a more detailed understanding of the complete three-dimensional velocity field. In cross section 1, two well-defined structures can be observed. On the left hand side, a pair of counterrotating vortices originating from the bronchi "U2" and "L2" can be found. On the right hand side, another pair of counterrotating vortices can be observed. These two vortices originate from the jets of the bronchi "U1" and "L1".

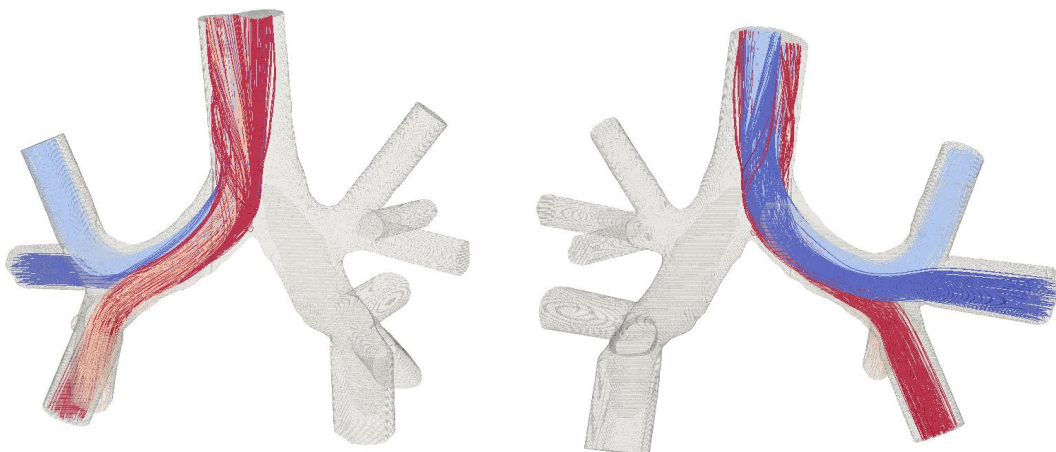


Fig. 10: Numerically determined streamlines at steady expiration.
Left: dorsal view. Right: ventral view.

In cross section 2 the movement of the vortex originating from the bronchus "L2" below the pair of counterrotating vortices on the ride hand side can be seen. A new vortical structure occurs at the upper part of the bronchus which is not captured by the experimental data. In cross section 3 the new formed vortex and the vortex of the bronchus "L2" have already vanished and the strength of the pair of counterrotating vortices decreases as well since the main movement of the fluid is in downstream direction. In cross section 4 the vortex originating from the bronchus "U1" can be hardly identified in the upper right corner of the cross section. All other in-plane fluid motions have vanished since the curvature of the bronchus in this part of the lung is too weak to generate or maintain vortical fluid motion.

In Fig. 10 the streamlines evidence the hypothesis that there is no pronounced mixing of the different fluid jets from the branches in the left main-bronchus. The fluid jets are still well-defined at the end of the bronchus and in the trachea a mixing and curling of the jets can be visible. The vortices do not form due to the curvature of the sub-bronchi to the main-bronchus or the curvature of the main-bronchus. The main reason of the rotation is the merging of the flows and the redirection of the jets. The sense of rotation of the vortices depends on the origin of the flow and the redirection in the main-bronchus due to the merging of four different jets.

5. Conclusions

The steady flow through the left main-bronchus of the upper airways of the human lung has been experimentally and numerically analyzed using particle-image velocimetry measurements and Lattice- Boltzmann simulations. The comparison of the velocity distributions has shown a convincing agreement of the numerical and experimental data.

The results show a counterrotating vortex pair caused by two jets originating from the sub-bronchi "U1" and "L1" to dominate the flow in the bronchus. The existence of those structures is not caused by the curved shape of the bronchus, i.e., it is not generated by the interaction of the viscous and centrifugal forces since the Dean number is too small. The vortices are excited by the merging of the jets which increases the shear stress distribution upstream of the bronchus. That is, the flow structures are excited by the converging flows of varying strength through the different bronchi and not by the curvature of the bronchus. All vortical structures vanish at the end of the bronchus due to the viscosity.

6. Acknowledgments

The funding of the 'Deutsche Forschungsgemeinschaft' in the frame of the joint program 'EXHALAT' is gratefully acknowledged. The authors are grateful for the computing resources provided by the High Performance Computing Center Stuttgart (HLRS).

References

- [1] C. D. Mathers and D. Loncar. Projections of global mortality and burden of disease from 2002 to 2030. *PLoS Med*, 3(11):442, 11 2006.
- [2] Z.L. Borrill, K. Roy, and D. Singh. Exhaled breath condensate biomarkers. *European Respiratory Journal*, 32(2):472–486, 2008.
- [3] G. Hillas, S. Loukides, K. Kostikas, and P. Bakakos. Biomarkers obtained by non-invasive methods in patients with copd: Where do we stand, what do we expect? *Current Medicinal Chemistry*, 16:2824–2838, 2009.
- [4] G. Eitel, T. Soodt, and W. Schröder. Investigation of pulsatile flow in the upper human airways. *Modelling in Medicine and Biology*, 1:147–165, 2011.
- [5] T. Soodt, F. Schröder, M. Klaas, T. van Overbrüggen, and W. Schröder. Experimental investigation of the transitional bronchial velocity distribution using stereo scanning PIV. *Experiments in Fluids*, 52(3):709–718, 2012.
- [6] Z. Zhang and C. Kleinstreuer. Airflow structure and nano-particles deposition in a human upper airway model. *Journal of Computational Physics*, 198:178–210, 2004.
- [7] Y. Zhang and W. H. Finlay. Experimental measurements of particle deposition in a proximal lung bifurcation models with an idealized mouth-throat. *Journal of Aerosol Medicine*, 18:460–473, 2005.
- [8] Z. Zhang and C. Kleinstreuer. Transient airflow structures and particle transport in a sequentially branching lung airway model. *Physics of Fluids*, 14:862–880, 2002.
- [9] F. E. Fresconi, A. S. Wexler, and A. K. Prasad. Expiration flow in a symmetric bifurcation. *Experiments in Fluids*, 35(5):493–501, 2003.
- [10] A. Ramuzat and M. L. Riethmuller. PIV investigation of oscillating flow with a 3d lung multiple bifurcations model. In *11th International Symposium on Applications of Laser Technique to Fluid Mechanics*, 2002.
- [11] E. R. Weibel. *Morphology of the human lung*. Academic, New York, 139, 1963.
- [12] F. E. Fresconi and A. K. Prasad. Secondary velocity fields in the conducting airways of the human lung. *Journal of Biomechanical Engineering*, 129:722–732, 2007.
- [13] K. Adler, W. Schröder, and Ch. Brücker. DPIV measurements of dynamic flow patterns in a realistic model of the lung airways down to the 6th generation. In *13th International Symposium on Applications of Laser Technique to Fluid Mechanics*, Lisbon, Portugal, June 26-29, 2006.
- [14] K. Bauer, A. Rudert, and Ch. Brücker. Three-dimensional flow patterns in the upper human airways. *Transactions of the ASME-K-Journal of Biomechanical Engineering*, 134(7):071006, 2012.
- [15] K. Adler and Ch. Brücker. Dynamic flow in a realistic model of the upper human lung. *Experiments in Fluids*, 4(2-3):411–423, 2007.
- [16] K. Horsfield, G. Dart, D. E. Olson, G. F. Filley, and G. Cumming. Models of the human bronchial tree. *Journal of Applied Physiology*, 31(2):207–217, 1971.

- [17] W. R. Dean. Fluid motion in a curved channel. *Proceedings of the Royal Society London A*, 121:402–420, 1928.
- [18] W. R. Dean and J. M. Hurst. Note in the motion of fluid in a curved pipe. *Mathematika*, 6:77–85, 1959.
- [19] T.B.Martonen, X.Guan, and R.M.Schreck. Fluid dynamics in airway bifurcation: II. secondary currents. *Inhalation Toxicology*, 13:281–289, 2001.
- [20] C. van Ertbruggen, C. Hirsch, and M. Paiva. Anatomically based three-dimensional model of airways to simulate flow and particle transport using computational fluid dynamics. *Journal of Applied Physiology*, 98:970–980, 2005.
- [21] S. Große, W. Schröder, and M. Klaas. Time-resolved PIV measurements of vortical structures in the upper human airways. *Topics in Applied Physics*, 112:33–51, 2007.
- [22] S. Große, W. Schröder, M. Klaas, A. Klöckner, and J. Roggenkamp. Time resolved analysis of steady and oscillating flow in the upper human airways. *Experiments in Fluids*, 42:955–970, 2007.
- [23] R. K. Freitas and W. Schröder. Numerical investigation of the three-dimensional flow in a human lung model. *Journal of Biomechanics*, 41:2446–2457, 2008.
- [24] Y. Agrawal, L. Talbot, and K. Gong. Laser anemometer study of flow development in curved circular pipes. *Journal of Fluid Mechanics*, 85:497–518, 1978.
- [25] J. A. C. Humphrey, H. Iacovides, and B. E. Launder. Some numerical experiments on developing laminar flow in circular-sectioned bends. *Journal of Fluid Mechanics*, 154:357–375, 1985.
- [26] N.-S. Cheng. Formula for the viscosity of a glycerol-water mixture. *Industrial & engineering chemistry research*, 47(9):3285–3288, 2008.
- [27] M. Ishikawa, K. Irabu, I. Teruya, and M. Nitta. PIV measurement of a contraction flow using micro-bubble tracer. In *The 6th International Symposium on Measurement Techniques for Multiphase Flows*, 2009.
- [28] G. König, K. Anders, and A. Frohn. A new light scattering technique to measure the diameter of periodically generated moving droplets. *Journal of Aerosol Science*, 17:157–167, 1986.
- [29] H. E. Albrecht, M. Borys, N. Damaschke, and C. Tropea. *Laser Doppler and Phase Doppler Measurement Techniques*. 2003.
- [30] N. Semidetnov and C. Tropea. Conversion relationships for multidimensional particle sizing techniques. *Measurement Science and Technology*, 15:112–118, 2004.
- [31] G. Eitel-Amor, M. Meinke, and W. Schröder. A lattice-Boltzmann method with hierarchically refined meshes. *Computers & Fluids*, 75:127–139, April 2013.
- [32] P. L. Bhatnagar, E. P. Gross, and M. Krook. A Model for Collision Processes in Gases. I. Small Amplitude Processes in Charged and Neutral One-Component Systems. *Phys. Rev.*, 94(3):511–525, 1954.
- [33] D. Hänel. *Molekulare Gasdynamik, Einführung in die kinetische Theorie der Gase und Lattice-Boltzmann-Methoden*. Springer-Verlag, 2004.

- [34] Y. H. Qian, D. D’Humières, and P. Lallemand. Lattice BGK Models for Navier-Stokes Equation. *Europhysics Letters (EPL)*, 17(6):479–484, February 1992.
- [35] I. Hörschler, Ch. Brücker, W. Schröder, and M. Meinke. Investigation of the impact of the geometry on the nose flow. *European Journal of Mechanics - B/Fluids*, 25(4):471–490, 2006.
- [36] I. Hörschler, W. Schröder, and M. Meinke. Comparison of steady and unsteady nasal cavity flow solutions for the complete respiration cycle. *Computational Fluid Dynamics Journal*, 15(3):354–377, 2006.
- [37] M. Bouzidi, M. Firdaouss, and P. Lallemand. Momentum transfer of a Boltzmann-lattice fluid with boundaries. *Physics of Fluids*, 13(11):3452–3459, 2001.